Self-Diffusion Studies in CuBTC by PFG NMR and MD Simulations

M. Wehring,[†] J. Gascon,[‡] D. Dubbeldam,[§] F. Kapteijn,[‡] R. Q. Snurr,[||] and F. Stallmach*,[†]

Fakultät für Physik und Geowissenschaften, Universität Leipzig, Linnèstraβe 5, 04103 Leipzig, Germany, Catalysis Engineering, ChemE, Delft University of Technology, Julianalaan 136, 2628 BL Delft, The Netherlands, Faculty of Science, University of Amsterdam, Nieuwe Achtergracht 166, 1018 WV Amsterdam, The Netherlands, and Chemical and Biological Engineering Department, Northwestern University, 2145 Sheridan Road, Evanston, Illinois 60208-3120

Received: March 11, 2010; Revised Manuscript Received: May 3, 2010

Self-diffusion and relaxation time studies of C_3 to C_6 hydrocarbons adsorbed in the microporous metal−organic framework CuBTC were performed by nuclear magnetic resonance (NMR) in the temperature range of 193−373 K. The presence of paramagnetic copper species in the solid CuBTC framework leads to short longitudinal (T_1) and transverse (T_2) relaxation times of the hydrocarbons with typical values of $T_1 \lesssim 10$ ms and $T_2 \lesssim 3$ ms. Under these conditions, pulsed field gradient (PFG) NMR self-diffusion studies could only be performed at short observation times using the primary spin echo sequence with high-intensity pulsed magnetic field gradients. The obtained temperature dependent self-diffusion coefficients were analyzed using an Arrhenius approach. The activation energies of the alkanes are in the range of 6.5−8.5 kJ/mol, increasing slightly with increasing number of carbon atoms. Significantly higher values were found for propene (13.2 kJ/mol) and 1-butene (15.0 kJ/mol). These tendencies are consistent with corresponding measurements of heats of adsorption and with data obtained in molecular dynamics (MD) simulations. The MD simulations show a strong dependence of the heat of adsorption and diffusion on loading and temperature. This is caused by the preferential adsorption of small alkanes such as propane and butane in the side pockets of the CuBTC structure at low loading and temperature.

Introduction

In the field of tailored nanoporous materials, metal organic frameworks (MOFs) have attracted a great deal of attention during the last years. MOFs are crystalline materials consisting of metal clusters and organic linkers. These compounds form a three-dimensional lattice with a high specific pore volume,[1] which opens up prospective applications[2−5] such as gas storage, heterogeneous catalysis, gas separation, and purification.

This study focuses on the MOF copper(II)benzene-1,3,5-tricarboxylate[4]($Cu_3(BTC)_2(H_2O)_3$; CuBTC), which was synthesized the first time by Chui et al.[6] and named HKUST-1. The topological properties of this MOF are well-known and characterized.[7,8] CuBTC has a three-dimensional pore structure with main pores which have a diameter of 9 Å, side pores with a diameter of 5 Å, and triangular shaped windows with a diameter of 3.5 Å. After the original synthesis and characterization of CuBTC, experimental studies focused on alternative synthesis routes and advanced applications[9−11] of this material.

Additionally, a large number of computer simulations were carried out in order to elucidate the host−guest interactions.[8,12−17] The adsorption behavior of gas mixtures in CuBTC was simulated by Yang et al.,[18] who investigated the prospective application of CuBTC for the separation of CO_2 from flue gases. Further studies deal with the separation of CO_2/CO, CO_2/CH_4 and of different hydrocarbons.[19−21] Besides the adsorption behavior, the mobility of these guest molecules inside the framework is often studied by molecular dynamics (MD) simulations.[22−24] Experimental adsorption measurements on CuBTC were carried out to study its potential for H_2/CH_4 storage,[25,26] olefin separation,[11,16,27] and separation of CO_2 from biogas.[28] Its suitability as a molecular sieve for the separation of different gas mixtures was, for example, investigated by Wang et al.[9] and Krungleviciute et al.[29]

Despite the importance of the molecular mobility of adsorbed guest molecules for such potential applications of MOFs, only a few experimental studies on the diffusion of guest molecules in MOFs are available. Pulsed field gradient (PFG) NMR was applied to determine the self-diffusion coefficients of methane, ethane, cyclohexane, and benzene in MOF-5.[30] Kortunov et al.[31] applied interference microscopy to measure the transport diffusion of methane in the manganese MOF $Mn(HCO_2)_2$, and Chmelik et al.[24] investigated recently the transport diffusion of different C_4 hydrocarbons in CuBTC by infrared microscopy.

NMR studies of molecules in CuBTC proved to be difficult, since the nuclear magnetic relaxation times (T_1 and T_2) are rather short, leading, for example, to poor signal-to-noise ratios in spin echo NMR diffusion studies[32,33] and large line width as observed in Xe NMR spectroscopy.[34] The reasons for these short relaxation times are the magnetic interaction of the nuclear spins of the adsorbed molecules with the electron spin of the copper species in the CuBTC framework. In the perfect CuBTC structure, neighboring Cu^{2+} ions within the paddle wheel structures form dimers with a total electron spin of $S = 1$. It was shown by electron paramagnetic resonance (EPR) investigations that real materials additionally contain copper monomers ($S = 1/2$) and extra-framework copper which contribute also to the paramagnetic behavior.[34]

* To whom correspondence should be addressed. E-mail: stallmac@physik.uni-leipzig.de.
[†] University of Leipzig.
[‡] Delft University of Technology.
[§] University of Amsterdam.
[||] Northwestern University.

10.1021/jp102212w
Published on Web 05/21/2010

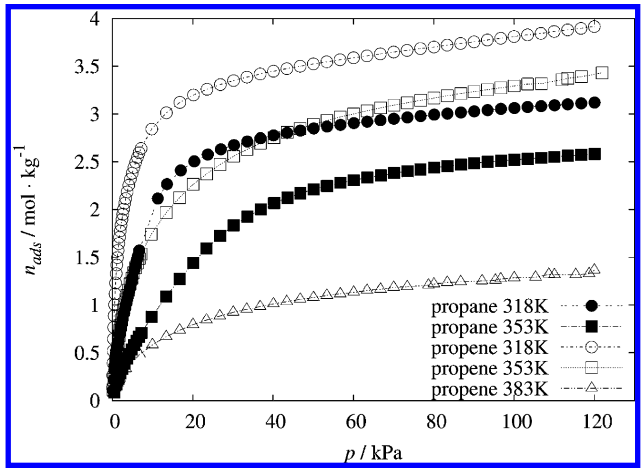

Figure 1. Adsorption of propane (filled symbols) and propene (open symbols) on CuBTC at 318, 353, and 383 K.

Nevertheless, in this work, we demonstrate that PFG NMR with the primary spin echo sequence, short observation times, and ultrahigh intensity magnetic field gradients is applicable for diffusion studies in CuBTC. Based on this method, we report experimental self-diffusion coefficients of C_3 to C_6 hydrocarbons in CuBTC at pore filling factors of about 25% in a temperature range of 193−373 K. Activation energies of self-diffusion, which are derived from these results, are discussed with respect to specific host−guest interactions. MD simulations were also performed and provide insights about the preferred adsorption locations within the MOF.

Materials and Methods

CuBTC Synthesis and Characterization. Copper(II) nitrate hydrate ($Cu(NO_3)_2 \cdot 3H_2O$) and 1,3,5- benzenetricarboxylic acid (trimesic acid) purchased from Aldrich were used as received, without further purification. Standard $Cu_3(BTC)_2$ crystals were prepared by the method described elsewhere:[1] 0.875 g (3.6 mmol) of $Cu(NO_3)_2 \cdot 3H_2O$ is dissolved in 12 mL of deionized water (solution A) and mixed with 0.42 g (2.0 mmol) of trimesic acid dissolved in 12 mL of ethanol (solution B). The resulting solution (A+B) is stirred for 30 min, placed in an autoclave, and heated under hydrothermal conditions (autogenous pressure) to 383 K for 18 h. Following this standard method, CuBTC crystals of an average size of 10 μm are synthesized (batch B). From our previous experience, we know that the final size of the CuBTC crystals depends on the concentration of the different reactants: the more concentrated the solution, the larger the crystals.[35] To this end, the concentrations of copper(II) nitrate hydrate and 1,3,5-benzenetricarboxylic acid in solutions A and B were concentrated (2 times) in order to produce larger crystals with an average diameter of 20 μm (batch A).

A Micromeritics ASAP 2010 gas adsorption analyzer (stainless steel version) was used to measure the adsorption isotherms (see Figure 1). Prior to the gas adsorption measurements, the samples were treated under vacuum at 423 K overnight in order to remove present solvents, moisture, and other volatile components. The crystalline materials were analyzed by X-ray diffraction (XRD) using a Bruker-AXS D5005 instrument with CuKα radiation using an internal (LaB_6) standard. Brunauer−Emmett−Teller (BET) surface areas of 1366 and 1250 m^2/g and micropore volumes of 0.55 and 0.53 cm^3/g were calculated from the N_2 adsorption isotherm at 77 K for the 10 and 20 μm crystals, respectively.

Figure 2 shows scanning electron microscope (SEM) images of representative crystals of both synthesis. The two batches

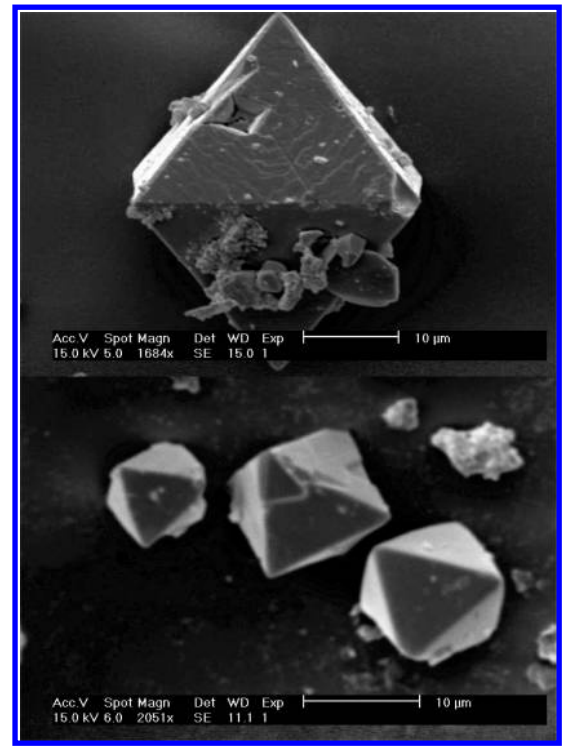

Figure 2. SEM images of large (batch A, on the top) and small (batch B, at the bottom) crystals of CuBTC.

consist of single crystals without agglomeration. However, the individual crystals exhibit some defects. Larger crystals are advantageous for NMR diffusion studies, since diffusional exchange with the surrounding gas phase does not influence the NMR measurements. Batch A (larger crystals) was used for NMR studies with adsorbed *n*-butane, 1-butene, *n*-pentane, and *n*-hexane. Batch B (smaller crystals) was used for NMR measurements with propane and propene only.

NMR Sample Preparation. For the NMR measurements, about 130 mg of the CuBTC samples was introduced into a NMR sample tube of 7.5 mm outer diameter and connected to a vacuum system. To completely remove water, residual solvents, and air from the pore structure, the samples were slowly heated under continuous evacuation up to a final temperature of 403 K, which was then maintained for at least 12 h. After this activation procedure, the samples were cooled down under vacuum to room temperature. Afterward, volumetrically determined amounts of the hydrocarbon gases and vapors were adsorbed onto the samples at the temperature of liquid nitrogen. Thus, the corresponding amounts of the hydrocarbons were frozen into the NMR sample tubes which finally were sealed by melting. A homogeneous distribution of the hydrocarbons across the bed of the CuBTC in the sample tubes was ensured by storing the sealed samples for at least 24 h at room temperature before the NMR measurements.

In order to achieve comparable pore filling of the CuBTC with the different hydrocarbons (propane, propene, *n*-butane, 1-butene, *n*-pentane, and *n*-hexane), samples were prepared in such a way that the loading corresponds to about 80 carbon atoms of the respective hydrocarbon per unit cell of the CuBTC. One unit cell consists of 16 formula units forming 4 large and 8 small cavities. For *n*-butane, 80 carbon atoms per unit cell corresponds to 140 mg of *n*-butane per gram of activated CuBTC and roughly 25% pore filling at room temperature.

NMR Measurements. The relaxation and self-diffusion of hydrocarbons in CuBTC was investigated experimentally by

proton (^{1}H) nuclear magnetic resonance. The measurements were carried out with the home-built NMR spectrometer FEGRIS 400 FT operating at 400 MHz ^{1}H resonance frequency.[36]

The longitudinal (T_1) and transverse (T_2) relaxation times were studied by the inversion recovery pulse sequence[37] and the CPMG pulse sequence,[38] respectively. The delay times in the inversion recovery sequence were varied between 0.1 ms up to 51.2 ms. The interecho spacing in the CPMG sequence was set to 0.125 ms. Generally, 32 scans were sufficient to obtain a good signal-to-noise ratio in these relaxation measurements. The relaxation times were obtained by corresponding single-exponential fits of the observed time dependencies of the NMR signal intensities.

Due to the copper(II), which is included in the CuBTC framework, the relaxation times of the adsorbed species are short (see section 3). This limits the accessible diffusion times (Δ) in the spin echo NMR diffusion studies using the PFG technique. In order to obtain NMR signals, which are representative for the adsorbed molecules, one needs to ensure that $\Delta < T_2, T_1$. Therefore, PFG NMR studies were performed with the primary spin echo sequence[33] using short diffusion times from 1.0 to 1.4 ms. In order to obtain a sufficient spin echo attenuation due to diffusion under these conditions, strong pulsed field gradients (maximal gradient intensity: $g = 30$ T/m) were applied. The duration of the gradient pulse was fixed in all experiments to $\delta = 0.4$ ms. For each diffusion time, the spin echo attenuation ψ was measured by successively increasing the gradient intensity up to the maximal value given above.

To determine the self-diffusion coefficient from the spin echo attenuation ψ, a single-exponential model was used,

$$\psi = \frac{M(b)}{M_0} = \exp(-bD) \qquad b = (\gamma\delta g)^2\left(\Delta - \frac{1}{3}\delta\right) \tag{1}$$

where $M(b)$ denotes the NMR signal intensity as function of the so-called b -value, which depends on the applied pulsed field gradients only.[39,33] Such a single exponential behavior was found for all measurements with the large CuBTC samples from batch A.

A slight indication for a multiexponential behavior of the spin echo attenuations was measured on the smaller crystals from batch B loaded with propane and propene. However, the signal-to-noise ratio in these measurements did not allow a reliable multiexponential analysis of these data. Therefore, we determined only the averaged self-diffusion coefficient using eq 1. The intracrystalline self-diffusion coefficients were measured by PFG NMR in the temperature range of 193−373 K. These data were analyzed in an Arrhenius plot yielding the pre-exponential factors D_0 and the activation energies E_A.

$$D(T) = D_0 \exp\left(-\frac{E_A}{RT}\right) \tag{2}$$

MC and MD Simulations. Monte Carlo (MC) and molecular dynamics (MD) simulations were carried out using a classical force field and a rigid framework for the CuBTC MOF. The positions of the framework were taken from the description of the crystal structure by Chui et al.[6] The force field Lennard−Jones parameters for the framework were taken from the DREIDING force field[40] except for the copper atom that was taken from the UFF force field.[41] The alkanes were modeled using the united-atom model with parameters taken from the TraPPE model.[42] The corresponding Lennard−Jones parameters are shown in Table 1.

TABLE 1: Lennard−Jones Parameters ε (Strength) and σ (Size) for the Framework Atoms and Adsorbates[40−42]

type	ε/k_B [K]	σ [Å]
Cu	2.518	3.114
O	48.19	3.03
C	47.86	3.47
H	7.65	2.85
CH_3	108.0	3.76
CH_2	56.0	3.96

MC simulations were used to compute the isosteric heats of adsorption. At the desired temperature, we performed two simulations: (1) a simulation of a single molecule inside the framework and (2) a simulation of a single molecule in the gas phase. We used translation, rotation, and reinsertion moves for 10^6 cycles. The isosteric heat of adsorption at infinite dilution is then computed as the average energy of simulation (1) minus the average energy of simulation (2) minus a factor k_BT.

Diffusion coefficients were obtained from MD simulations. In MD simulations,[43−45] successive configurations of the system are generated by integrating Newton's laws of motion, which then yields a trajectory that describes the positions, velocities, and accelerations of the particles as they vary with time. We used the velocity Verlet integration scheme with a time step of 0.5 fs. The potentials were shifted to zero at the cutoff of 12 Å. Temperature control was realized by using the Nose−Hoover−Chain thermostat algorithm.[46] The self-diffusion coefficients were obtained from the slope of the mean-squared displacement versus time using an order-n algorithm.[44,47]

The MD simulations started with randomly placing the alkane chains into the framework. The positions were then equilibrated using MC simulations with translation, rotation, and reinsertion moves for 10^4 cycles. Next, velocities were assigned from the Maxwell−Boltzmann distribution and the MD equilibration phase started. After equilibration, the production run started, during which we measured the diffusion coefficients. The production runs were longer than 150 ns for all simulations. Energy conservation and thermal control were excellent.

To gain additional insight into diffusion behavior, long MD simulations at a fixed loading of 20 molecules per unit cell for C_1 to C_6 n-alkanes at 300 K were performed. We started with all of the molecules inside the main channels and equilibrated. After the equilibration, we measured what percentage of these molecules were inside the small side pockets (and what percentage in the main channels), how long the molecules stayed inside the pockets, and the self-diffusion coefficients. The criterion whether a molecule was inside a small pocket or in the main channel was chosen as whether the most central bead of an alkane was within a radius of 5 Å from any center of a pocket.

To support the NMR relaxation time studies, the dynamics of rotation of n-butane, n-pentane, and n-hexane was studied by MD simulations using the approach of Saengsawang et al.[48] The autocorrelation function of the orientation dependent factor of the dipolar interaction $A(t) = (5/8)^{1/2}(3\cos^2\theta(t) - 1)$ was calculated, where θ is the angle between the molecular end-to-end vector and the MOF coordinate system. While Saengsawang et al. fitted the autocorrelation function to a function with three exponential components, we used the time τ at which the autocorrelation function has dropped down to $1/e$ as characteristic averaged time of rotational reorientation of the molecule.

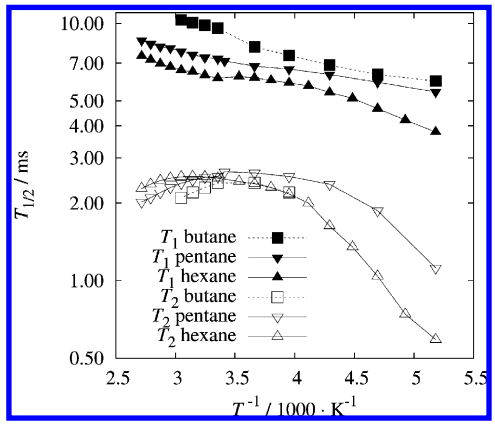

Figure 3. Longitudinal (T_1) and transverse (T_2) relaxation times of *n*-alkanes adsorbed in CuBTC.

This time constant τ is used as correlation time to estimate NMR relaxation times, which are compared with the experimental data from NMR measurements.

Results and Discussion

Figure 1 shows the single component adsorption isotherms for propane and propylene measured over a temperature range of 318−383 K. As it can be observed, propene adsorbs stronger in CuBTC than propane. The adsorption isotherms were analyzed using a one site Langmuir adsorption model, which yielded heats of adsorption of 31 kJ/mol for propane and 43 kJ/mol for propene, in good agreement with those measured by Wagener et al.[49] In a previous work,[8] we showed a good agreement between our measured isotherms and those calculated at low temperatures. However, only poor agreement was achieved at the higher temperatures, where simulations provided much higher adsorption capacities than those obtained experimentally. The negative thermal expansion of the MOF framework, which was shown by Wu et al.[50] for CuBTC, might be a possible explanation for this discrepancy at high temperatures.

Figure 3 shows the longitudinal and the transverse relaxation times for *n*-butane, *n*-pentane, and *n*-hexane in CuBTC. The longitudinal relaxation time increases monotonously with increasing temperature, which means that the correlation time of the reorientation of the adsorbed molecules due to thermal motion is short compared with the inverse of the NMR Larmor frequency of $1/(2\pi f_L) = 4 \times 10^{-10}$ s. This is typical for a liquidlike behavior.[51] In this motional regime, one expects for free liquids that $T_2 \leq T_1$, which is in fact observed for these adsorbates. Compared to zeolitic adsorbate−adsorbent systems,[52] both of the relaxation times are rather short ($T_1 \leq 10$ ms, $T_2 \leq 3$ ms).

The averaged correlation times of rotational reorientation τ calculated by the MD simulations range from 0.5×10^{-12} s for *n*-butane to 2.0×10^{-12} s for *n*-hexane at room temperature (Table 2). They are more than 2 orders of magnitude shorter than the inverse of the NMR Larmor frequency, calculated above. Based on the Bloembergen-Purcell-Pound (BBP) theory,[53] the longitudinal relaxation time of a molecule in this fast motional averaging regime may be estimated. For adsorbed hydrocarbons in CuBTC, it is reasonable to assume that the longitudinal relaxation rate ($1/T_1$) results from relaxation due to spin rotation interaction ($1/T_{1,SR}$) between the ^{1}H nuclear spins and the angular momentum of the molecule, intramolecular dipole−dipole interaction ($1/T_{1,intra}$) between the ^{1}H spins within a single molecule and due to paramagnetic interaction ($1/T_{1,para}$) with the electron spins of framework and extra-framework copper species. Intermolecular dipole−dipole interactions between the ^{1}H nuclei are usually much smaller than the intramolecular, spin rotation, and paramagnetic interactions and will, therefore, be disregarded in this estimation. The total relaxation rate is thus given by[54]

$$\frac{1}{T_1} = \frac{1}{T_{1,intra}} + \frac{1}{T_{1,SR}} + \frac{1}{T_{1,para}} \quad (3)$$

Using the approach of Oosting and Trappeniers[54] to determine $T_{1,intra}$ (eq 12 in ref 54) and $T_{1,SR}$ (eq 22 in ref 54) and adding the corresponding rates to calculate a longitudinal relaxation time by disregarding the relaxation due to paramagnetic interaction, we estimated a value of approximately 190 ms for *n*-butane at room temperature. Since this value is much larger than the experimental T_1 relaxation time for *n*-butane (10 ms), it can be concluded that the paramagnetic interaction has a significant influence on the relaxation process. Such a strong influence of paramagnetic species on proton (^{1}H) nuclear magnetic relaxation times is well-known for bulk liquids. Obviously, the paramagnetic interactions shorten the relaxation times of the *n*-alkanes in the CuBTC framework significantly.

These short T_1 and T_2 relaxation times limit the observation times Δ and the duration of the pulsed field gradients δ for the PFG NMR self-diffusion studies. Therefore, the diffusion measurements were performed with the primary spin echo sequence as we discussed in section 2. Note that the transverse and longitudinal relaxation times for *n*-hexane are rapidly shrinking for temperatures below 233 K. Thus, it becomes impossible to perform the PFG NMR studies at these low temperatures.

The measured spin echo attenuation curves show a monoexponential behavior for all guest molecules adsorbed in crystals of the batch A. A representative example is shown in Figure 4, which displays the spin echo attenuations for *n*-pentane for different observation times and temperatures. The monoexponential decay indicates a homogeneous mobility of the guest molecules inside the crystals. Only for propane and propene

TABLE 2: Activation Energies and Pre-Exponential Factors for the Self-Diffusion of Hydrocarbons Adsorbed in CuBTC (Batch A and B), Isosteric Heats of Adsorption (Experimental ΔH_{exp} and Computer Simulated ΔH_{sim} Values) Compared with Literature Data, and Characteristic Averaged Times of Rotational Reorientation τ Obtained by Computer Simulations

				$-\Delta H_{exp}$ (kJ/mol)		$-\Delta H_{sim}$ (kJ/mol)		τ (ps)
batch	adsorbate	D_0 (m^2/s)	E_A (kJ/mol)	this work	ref	this work	ref	this work
B	propane	2.4×10^{-9}	6.5	31	30[49]	49	49[8]	
B	propene	2.7×10^{-8}	13.3	43	33[49]			
A	*n*-butane	2.3×10^{-8}	8.5		36[59]	56	29−57[59,24]	0.5
A	1-butene	3.2×10^{-8}	15.0		46 (*i*-butene)[11]			
A	*n*-pentane	9.9×10^{-9}	8.0			57		1.1
A	*n*-hexane	4.2×10^{-9}	8.2			56		2.0

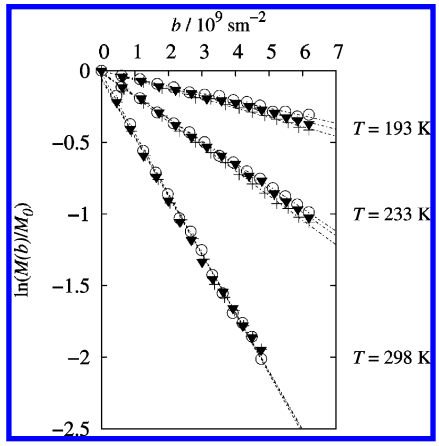

Figure 4. Spin echo attenuation of *n*-pentane adsorbed in CuBTC for different diffusion times (Δ = 1.0 (▼), 1.2 (+), 1.4 (○) ms) and different temperatures.

adsorbed in batch B a slight indication of a multiexponential behavior was found.

All PFG NMR spin echo attenuation curves are independent of the diffusion time which was varied between 1.0 and 1.4 ms (see Figure 4). Thus, it appears that during this short time scales the external crystal surfaces do not hinder the motion of the guest molecules. This is confirmed by the diffusion length of almost 3 μm, which is small compared to the size of the crystals of about 20 μm. The described monoexponential behavior and diffusion time independence of the attenuation curves were observed at all temperatures (see Figures 4 and 5). It was found that the mobility of the guest molecules increases with increasing temperature, as easily seen in the increasing decays of the attenuation curves (Figures 4 and 5).

Figure 5 shows the comparison of the spin echo attenuation curves of the saturated *n*-butane and the unsaturated 1-butene. As discussed above, the curves show also a monoexponential behavior over the whole temperature range. The unsaturated 1-butene shows a significantly slower decay than the saturated *n*-butane. This is a direct evidence for a smaller diffusivity of the unsaturated hydrocarbon at the same temperature. In agreement with reports on corresponding differences in isosteric heats of adsorption,[11] this is caused by the interaction of the π electrons with the CuBTC framework. The self-diffusion coefficients, which are determined by eq 1, are 7.3×10^{-10} m^2/s for *n*-butane and 6.7×10^{-11} m^2/s for 1-butene at room temperature.

Figure 6 shows the temperature dependent self-diffusion coefficients of *n*-butane, 1-butene (Figure 6a), *n*-pentane, and *n*-hexane (Figure 6b) in an Arrhenius presentation. The determined values for the activation energies of the self-diffusion are about 8 kJ/mol for the saturated alkanes. The unsaturated 1-butene exhibits a significantly higher activation energy of 15 kJ/mol. The same trend of a strongly increased activation energy for the unsaturated hydrocarbon was also observed for propane and propene in batch B (see Table 2). However, the activation energies are just slightly lower than those of the corresponding C_4 hydrocarbons (propane, 6.5 kJ/mol; propene, 13.3 kJ/mol).

It is also remarkable that the pre-exponential factors of the self-diffusion of the *n*-alkanes (C_6 to C_4) decrease with increasing chain length (see Table 2). Only the pre-exponential factors

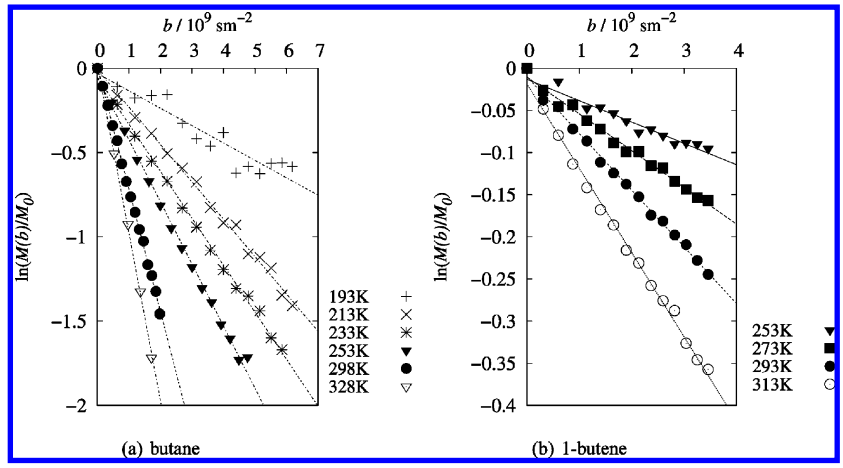

Figure 5. Spin echo attenuation of (a) *n*-butane and (b) 1-butene adsorbed in CuBTC (batch A) for different temperatures.

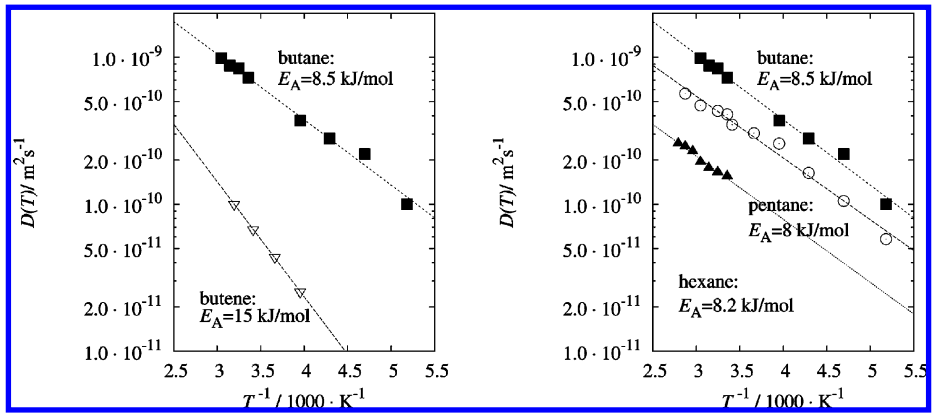

Figure 6. Intracrystalline self-diffusion coefficients of *n*-butane (■), 1-butene (▽) (left) and *n*-butane (■), *n*-pentane (○), *n*-hexane (▲) (right), with the corresponding activation energies of self-diffusion.

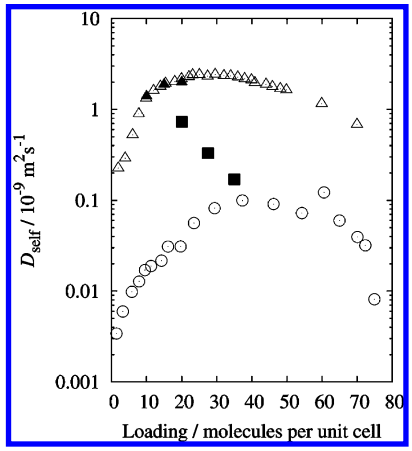

Figure 7. Self-diffusion coefficients of *n*-butane at room temperature obtained by PFG NMR (■, this work) and by molecular dynamics simulations (▲, this work; △, Supporting Information of ref 24). Maxwell−Stefan diffusivities of *n*-butane at room temperature measured by infrared microscopy (○, ref 24).

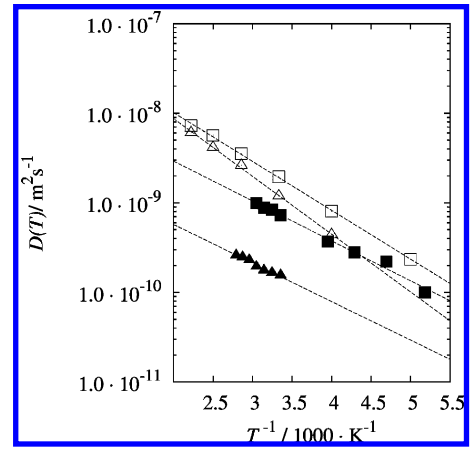

Figure 8. Intracrystalline self-diffusion coefficients of *n*-butane (□,■) and *n*-hexane (△,▲) obtained by PFG NMR (filled symbols) and MD simulations (open symbols). The corresponding activation energies of self-diffusion measured by PFG NMR are 8.5 kJ/mol for *n*-butane and 8.2 kJ/mol for *n*-hexane. The results for the MD-simulations are 10.4 kJ/mol for *n*-butane and 12.3 kJ/mol for *n*-hexane. The PFG NMR measurements and the MD simulations are performed with a loading of 20 molecules per unit cell.

for propane and propene are not found to be significantly larger that those of the C_4 hydrocarbons. Note that the NMR measurements with the C_3 hydrocarbons were performed on a different CuBTC batch (B) which might explain this finding. The measured activation energies (E_A) and pre-exponential factors (D_0) are given in Table 2. The data for the activation energies are compared with available literature data for isosteric heats of adsorption (experimental and computer simulated values). The experimental value of the isosteric heats of adsorption are also higher for the unsaturated hydrocarbons than for the saturated ones with differences which are in the same order of magnitude as the corresponding differences of the activation energies of diffusion. The pre-exponential factors for the *n*-alkanes loaded at batch A show the expected trend (decreasing D_0-values with increasing chain length). Only propane in batch B does not follow this expected trend, which might be caused by the different synthesis conditions.

For a deeper understanding of the measured diffusion behavior, the experimental loading and temperature dependent self-diffusion coefficients were directly compared with the computer simulated data. Figure 7 compares the loading dependence of the intracrystalline self-diffusion coefficient of *n*-butane measured with PFG NMR (this work) with data obtained by MD simulation (this work and Supporting Information of ref 24) and Maxwell−Stefan diffusivities, obtained from transport diffusion measurements by IR microscopy.[24] Depending on the loading, the self-diffusion coefficients measured via PFG NMR are up to an order of magnitude slower than the computer simulated values but faster than the experimental Maxwell−Stefan diffusivities. For a loading of 35 molecules per unit cell, the values from PFG NMR are in good agreement with the Maxwell−Stefan diffusion coefficients extracted from IR microscopy. However, for decreasing loadings, the PFG NMR data show an opposite trend compared to the results of the MD simulations and the IR microscopy.

The temperature dependent diffusivities of *n*-butane and *n*-hexane obtained by PFG NMR and MD simulations at a small loading of about 20 molecules per unit cell (see Figure 8) show only a slight disagreement between MD simulation and experiment. The experimental data for the *n*-butane diffusivities are about a factor of 3 smaller than the MD simulation results, and the activation energies differ by about 2 ± 1 kJ/mol. This value does not significantly exceed the experimental uncertainties. For *n*-hexane, the experimental data are about a factor of 8 smaller than the MD data and the difference in activation energy is 4 ± 1.5 kJ/mol. Please note that the short transverse relaxation times for *n*-hexane permitted us to obtain experimental diffusion data only over a narrow range of temperatures which increases the experimental uncertainty of this value. It is also remarkable that the pre-exponential factors of self-diffusion of *n*-butane and *n*-hexane are the same for the MD simulations ($(1.5 \pm 0.2) \times 10^{-7}$ m^2/s) while the experimental data are much smaller (see Table 2) with an additional significant difference between the values for *n*-butane and *n*-hexane.

The MD result means that in an ideal CuBTC crystal at infinite temperatures *n*-butane and *n*-hexane should feel the same steric restrictions due to the same pore network topology. As the comparison with the experimental data suggests, in a real CuBTC crystal, this is obviously not the case. While the similar activation energies point toward a fairly good representation of the interaction potentials between the adsorbates and the CuBTC framework in the MD simulations, the restrictions due to real pore topology are not well represented. These obstructions of the diffusion due to the real pore topology must be sought in deviations from the ideal CuBTC crystal structure, which do not enter into the MD simulations but affect the experimental PFG NMR diffusion studies. It could be possible that a part of the micropores are blocked by residual solvents, copper species not incorporated in the CuBTC framework, or local defects in the crystal structure. Such extra-framework copper species in CuBTC were also observed by Hartmann et al.[11] Additionally, it cannot be excluded that crystal defects in the CuBTC MOF create internal diffusion barriers. Recently, Karwacki[55] reported the formation of such internal barriers for zeolites by small angle mismatches between neighboring crystal areas. Since the experimental intracrystalline diffusion data are independent of observation time, such internal barriers must be homogeneously distributed over length scales smaller than the observed rms displacements (about 3 μm). Their permeability must be lower for *n*-hexane compared to *n*-butane in order to account for the difference in the experimental pre-exponential factors.

Volume changes in MOFs, which are reported by Ramsahye et al.[56] for MIL-53 and MIL-47 and which should also occur in CuBTC due to its negative thermal expansion,[8,57] could also account for the difference between the pre-exponential factors

TABLE 3: Properties of Linear Alkanes in CuBTC at 300 K and 20 Molecules per Unit Cell from MD Simulations

type	run time (ns)	percentage in pockets (%)	max residence time (ns)	D_{self} (m^2/s)
C_1	1073	44.8 ± 0.5	0.5	18.0×10^{-9}
C_2	1073	42.5 ± 1.7	5	6.7×10^{-9}
C_3	845	39.5 ± 11.4	>20	3.3×10^{-9}
n- C_4	648	38.1 ± 9.5	>20	2.1×10^{-9}
n- C_5	543	33.5 ± 4.6	15	1.6×10^{-9}
n- C_6	450	28.9 ± 5.2	7.5	1.2×10^{-9}

observed in the NMR experiment and the MD simulations. While the MD simulations do not yet take into account a decreasing lattice constant with increasing temperature, its influence is naturally present in the temperature dependent experimental data. It should also be noted that the MD simulations are performed with a rigid framework. The flexibility of the framework is expected to have some influence on the mobility of guest molecules as reported by Greathouse and Allendorf.[58]

Additionally, due to the pore topology of the CuBTC consisting of large main and smaller side pores, the results of the computer simulations for heats of adsorption and self-diffusion depend strongly on the occupancy, and MD simulations of self-diffusion need to be performed with very long runs. To illustrate this, Table 3 compares the residence times and the relative occupancy of the C_1 to C_6 alkanes in the small pockets at 300 K and a loading of 20 molecules per unit cell. The simulations for methane were run for more than a microsecond, and around 45% of the molecules were inside the small pockets. This value should be compared to 8/20, where 8 is the number of pockets and 20 the number of molecules per unit cell. If all of the pockets are filled with a single molecule, one would expect 40% occupancy. For methane and ethane, the observed result is slightly higher. Most, if not all, pockets are filled, and more than one molecule of methane and ethane per pocket is possible (using our pocket criterion). Ethane stays an order of magnitude longer in the side pockets than methane. This trend continues for propane and butane, which were too long to reliably measure. From pentane onward, the additional alkane beads stick out of the pocket, which makes hopping in and out of the pockets much easier. Our results point to a very tight fit of propane and butane in the pockets. The occupancy of the side pockets, however, depends on temperature, and very large differences in heat of adsorption can be obtained.[59] At low temperature, the high heat of adsorption of the small pockets is measured, while at high temperature the lower heat of adsorption of the main channels is probed. At higher temperatures, propane and butane are driven out of pockets and into the main channel. A similar effect on the heat of adsorption can be observed as a function of loading.[24] In Figure 7a of ref 24, one can observe at low loading a high heat of adsorption from the small pockets and at higher loading a bigger contribution from the main channel which has a much lower heat of adsorption. Because at fixed loading a roughly similar fraction of molecules is found inside the small pockets as a function of chain length (16−18 molecules per unit cell), the diffusion coefficients mainly involve the fast moving fraction. Therefore, the usual decay of self-diffusivity with chain length is observed in Table 3.

From this initial study, we found that very long simulations are needed to reliably calculate diffusion coefficients in CuBTC. In very short simulations, there are "fast" and "slow" molecules (molecules that are outside and inside the small pockets). Only after sufficiently long runs, reliably averaged results are obtained. This also has implications for the comparison and interpretation of simulation versus experimental results, where the differences in the time scales between NMR experiments and MD simulations are about 3 orders of magnitude. With such a tight fit of molecules in side pockets, differences are to be expected.

Conclusion

We have demonstrated the ability of the PFG NMR technique to measure the temperature and loading dependent intracrystalline self-diffusion coefficients of short *n*-alkanes and alkenes adsorbed in the MOF CuBTC. Despite the difficulties due to paramagnetic copper species in the CuBTC framework, the PFG NMR data obtained are self-consistent, yielding experimental values for the intracrystalline self-diffusion. These data were compared with results from MD simulations. The simulated self-diffusion coefficients are generally larger than the experimental values. The reason for this discrepancy is most likely deviations from the ideal crystal structure which influence the experimental data but are not taken into account in the MD simulations. The simulations suggest that small alkanes such as propane and butane fit snugly into the side pockets of the CuBTC structure. These pockets are preferential sites at low loading and temperature. The ratio of particles inside the pockets versus the main channels and therefore the heat of adsorption results are extraordinarily sensitive to temperature and loading. The residence times of the tight fitting molecules is on the order of many nanoseconds, and only after sufficiently long simulations reliable results for diffusion data can be obtained. The large scatter in CuBTC literature results, between simulation and experiment, and between different experiments, can also be attributed to this structural sensitivity and whether the pockets are accessible.

From the measured temperature dependent self-diffusion coefficients, the activation energies were determined. For the *n*-alkanes, they agree within the experimental uncertainty with the corresponding values from MD simulations. The activation energies increase by about 7 kJ/mol for alkenes compared to the alkanes with the same number of carbon atoms. The different trends in loading dependence remain an unresolved issue. While NMR shows that the self-diffusion coefficient decreases with increasing loading, MD simulations and experimental data from transport diffusion studies by IR microscopy show that there should be a maximum of mobility at intermediate pore fillings.

Acknowledgment. We thank the German, the Dutch, and the U.S. science foundations DFG, NWO, and NSF for financial support via the International Research Training Group "Diffusion in porous materials", the DFG Grant STA 648/1-1 and the NSF Grant CTS-0507013. J.G. gratefully acknowledges The Netherlands National Science Foundation (NWO) for his personal VENI grant and Senter Novem for financial support through the "EOS-LT Consortium Anorganische Membraan Technologie" (Lange termijn EOS-onderzoeksprogramma's), EOSLT04008 managed by ECN.

Nomenclature

D	self-diffusion coefficient
D_0	pre-exponential factor
E_A	activation energy
g	pulsed gradient intensity
k_B	Bolzmann constant
R	universal gas constant
T	temperature in Kelvin

γ	gyromagnetic ratio
δ	pulsed gradient duration
Δ	observation time
τ	characteristic time of rotational reorientation
ψ	spin echo attenuation

References and Notes

(1) Schlichte, K.; Kratzke, T.; Kaskel, S. *Microporous Mesoporous Mater.* **2004**, *73*, 81–88.

(2) Mueller, U.; Schubert, M.; Teich, F.; Puetter, H.; Schierle-Arndt, K.; Pastre, J. *J. Mater. Chem.* **2006**, *16*, 626–636.

(3) Gascon, J.; Aktay, U.; Hernandez-Alonso, M. D.; van Klink, G. P. M.; Kapteijn, F. *J. Catal.* **2009**, *261*, 75–87.

(4) Gascon, J.; Hernandez-Alonso, M. D.; Almeida, A. R.; van Klink, G. P. M.; Kapteijn, F.; Mul, G. *ChemSusChem* **2008**, *1*, 981–983.

(5) Couck, S.; Denayer, J. F. M.; Baron, G. V.; Remy, T.; Gascon, J.; Kapteijn, F. *J. Am. Chem. Soc.* **2009**, *131*, 6326.

(6) Chui, S. S.-Y.; Lo, S. M.-F.; Charmant, J. P.; Orpen, A. G.; Williams, I. D. *Science* **1999**, *283*, 1148–1150.

(7) Prestipino, C.; Regli, L.; Vitillo, J. G.; Bonino, F.; Damin, A.; Lamberti, C.; Zecchina, A.; Solari, P. L.; Kongshaug, K. O.; Bordiga, S. *Chem. Mater.* **2006**, *18*, 1337–1346.

(8) Garcia-Perez, E.; Gascon, J.; Morales-Florez, V.; Castillo, J. M.; Kapteijn, F.; Calero, S. *Langmuir* **2009**, *25*, 1725–1731.

(9) Wang, Q. M.; Shen, D. M.; Bulow, M.; Lau, M. L.; Deng, S. G.; Fitch, F. R.; Lemcoff, N. O.; Semanscin, J. *Microporous Mesoporous Mater.* **2002**, *55*, 217–230.

(10) Guo, H.; Zhu, G.; Hewitt, I. J.; Qiu, S. *J. Am. Chem. Soc.* **2009**, *131*, 1646–1647.

(11) Hartmann, M.; Kunz, S.; Himsl, D.; Tangermann, O.; Ernst, S.; Wagener, A. *Langmuir* **2008**, *24*, 8634–8642.

(12) Vishnyakov, A.; Ravikovitch, P. I.; Neimark, A. V.; Bulow, M. *Abstr. Pap. Am. Chem. Soc.* **2003**, *226*, 071INOR.

(13) Karra, J. R.; Walton, K. S. *Langmuir* **2008**, *24*, 8620–8626.

(14) Liu, J. C.; Culp, J. T.; Natesakhawat, S.; Bockrath, B. C.; Zande, B.; Sankar, S. G.; Garberoglio, G.; Johnson, J. K. *J. Phys. Chem. C* **2007**, *111*, 9305–9313.

(15) Wang, S. Y. *Energy Fuels* **2007**, *21*, 953–956.

(16) Nicholson, T. M.; Bhatia, S. K. *Adsorpt. Sci. Technol.* **2007**, *25*, 607–619.

(17) Yazaydin, A. O.; Benin, A. I.; Faheem, S. A.; Jakubczak, P.; Low, J. J.; Willis, R. R.; Snurr, R. Q. *Chem. Mater.* **2009**, *21*, 1425–1430.

(18) Yang, Q. Y.; Xue, C. Y.; Zhong, C. L.; Chen, J. F. *AIChE J.* **2007**, *53*, 2832–2840.

(19) Wang, S. Y.; Yang, Q. Y.; Zhong, C. L. *Sep. Purif. Technol.* **2008**, *60*, 30–35.

(20) Chen, D.; Zhang, L.; Liu, Y. C.; Wang, Q. *Acta Chim. Sin.* **2008**, *66*, 2227–2234.

(21) Martin-Calvo, A.; Garcia-Perez, E.; Castillo, J. M.; Calero, S. *Phys. Chem. Chem. Phys.* **2008**, *10*, 7085–7091.

(22) Skoulidas, A. I.; Sholl, D. S. *J. Phys Chem. B* **2005**, *109*, 15760–15768.

(23) Sholl, D. S. *Acc. Chem. Res.* **2006**, *39*, 403–411.

(24) Chmelik, C.; Kärger, J.; Wiebcke, M.; Caro, J.; van Baten, J.; Krishna, R. *Microporous Mesoporous Mater.* **2009**, *117*, 22–32.

(25) Krawiec, P.; Kramer, M.; Sabo, M.; Kunschke, R.; Frode, H.; Kaskel, S. *Adv. Eng. Mater.* **2006**, *8*, 293–296.

(26) Senkovska, I.; Kaskel, S. *Microporous Mesoporous Mate.* **2008**, *112*, 108–115.

(27) Jorge, M.; Lamia, N.; Rodrigues, A. *Colloids Surf., A* **2010**, *357*, 27−34.

(28) Cavenati, S.; Grande, C. A.; Rodrigues, A. E. *Ind. Eng. Chem. Res.* **2008**, *47*, 6333–6335.

(29) Krungleviciute, V.; Lask, K.; Migone, A. D.; Lee, J. Y.; Li, J. *AIChE J.* **2008**, *54*, 918–923.

(30) Stallmach, F.; Gröger, S.; Künzel, V.; Kärger, J.; Yaghi, O. M.; Hesse, M.; Müller, U. *Angew. Chem., Int. Ed.* **2006**, *45*, 2123–2126.

(31) Kortunov, P. V.; Heinke, L.; Arnold, M.; Nedellec, Y.; Jones, D. J.; Caro, J.; Karger, J. *J. Am. Chem. Soc.* **2007**, *129*, 8041–8047.

(32) Künzel, V. Diploma thesis, Universität Leipzig, 2005.

(33) Stallmach, F.; Galvosas, P. Spin echo NMR diffusion studies. *Annual Reports on NMR Spectroscopy*; Elsevier: Amsterdam, Boston, Heidelberg, 2007; Vol.61, pp 51−131.

(34) Boehlmann, W.; Poeppl, A.; Sabo, M.; Kaskel, S. *J. Phys Chem. B* **2006**, *110*, 20177–20181.

(35) Gascon, J.; Aguado, S.; Kapteijn, F. *Microporous Mesoporous Mater.* **2008**, *113*, 132–138.

(36) Kärger, J.; Bär, N.-K.; Heink, W.; Pfeifer, H.; Seiffert, G. *Z. Naturforsch.* **1995**, *50A*, 186.

(37) Banci, L.; Bertini, I.; Luchinat, C. *Nuclear and Electron Relaxation. The Magnetic Nucleus-Unpaired Electron Coupling in Solution*; VHC: New York, 1991.

(38) Carr, H. Y.; Purcell, E. M. *Phys. Rev.* **1954**, *94*, 630–638.

(39) Tanner, J. E. *J. Chem. Phys.* **1970**, *52*, 2523.

(40) Mayo, S. L.; Olafson, B. D.; Goddard, W. A. *J. Chem. Phys.* **1990**, *94* (26), 8897–8909.

(41) Rappe, A. K.; Casewit, C. J.; Colwell, K. S.; Goddard, W. A.; Skiff, W. M. *J. Am. Chem. Soc.* **1992**, *114* (25), 10024–10035.

(42) Martin, M.; Siepmann, J. *J. Am. Chem. Soc.* **1997**, *119* (38), 8921–8924.

(43) Allen, M. P.; Tildesley, D. J. *Computer Simulation of Liquids*; Clarendon Press: Oxford, UK, 1987.

(44) Frenkel, D.; Smit, B. *Understanding Molecular Simulation*; Academic Press: San Diego, 1996.

(45) Rapaport, D. C. *The Art of Molecular Dynamics Simulation*, 2nd ed.; Cambridge University Press: Cambridge, 2004.

(46) Martyna, G. J.; Tuckerman, M. E.; Tobias, D. J.; Klein, M. L. *Mol. Phys.* **1996**, *87*, 1117–1157.

(47) Dubbeldam, D.; Ford, D. C.; Ellis, D. E.; Snurr, R. Q. *Mol. Simul.* **2009**, *35*, 1084–1097.

(48) Saengsawang, O.; Schuring, A.; Remsungnen, T.; Loisruangsin, A.; Hannongbua, S.; Magusin, P. C. M. M.; Fritzsche, S. *J. Phys. Chem. C* **2008**, *112*, 5922–5929.

(49) Wagener, A.; Schindler, M.; F., R.; Ernst, S. *Chem. Ing. Tech.* **2007**, *79* (6), 851–855.

(50) Wu, Y.; Kobayashi, A.; Halder, G. J.; Peterson, V. K.; Chapman, K. W.; Lock, N.; Southon, P. D.; Kepert, C. J. *Angew. Chem., Int. Ed.* **2008**, *47*, 8929–8932.

(51) Bloembergen, N. *Nuclear Magnetic Relaxation*; W. A. Benjamin, Inc.: New York, 1961.

(52) Kärger, J.; Pfeifer, H.; Rauscher, M.; Walter, A. *J. Chem. Soc., Faraday Trans.* **1980**, *76*, 717–737.

(53) Bloembergen, N.; Purcell, E. M.; Pound, R. V. *Phys. Rev.* **1948**, *73*, 679–712.

(54) Oosting, P. H.; Trappeniers, N. J. *Physica* **1971**, *51*, 395–417.

(55) Karwacki, L.; et al. *Nat. Mater.* **2009**, 1–7.

(56) Ramsahye, N. A.; Maurin, G.; Bourrelly, S.; Llewellyn, P. L.; Serre, C.; Loiseau, T.; Devic, T.; Ferey, G. *J. Phys. Chem. C* **2008**, *112*, 514–520.

(57) Dubbeldam, D.; Walton, K. S.; Ellis, D. E.; Snurr, R. Q. *Angew. Chem., Int. Ed.* **2007**, *46*, 4496–4499.

(58) Greathouse, J. A.; Allendorf, M. D. *J. Phys. Chem. C* **2008**, *112*, 5795–5802.

(59) Farrusseng, D.; Daniel, C.; Gaudillere, C.; Ravon, U.; Schuurman, Y.; Mirodatos, C.; Dubbeldam, D.; Frost, H.; Snurr, R. Q. *Langmuir* **2009**, *25*, 7383–7388.

JP102212W